BULLETIN OF THE POLISH ACADEMY OF SCIENCES
TECHNICAL SCIENCES, Vol. 68, No. 3, 2020
DOI: 10.24425/bpasts.2020.133382

Vibration analysis of ball bearing considering waviness under high speed and an axial load

P.P. HOU[1], L.Q. WANG[1,2]*, and Q.Y. PENG[3]

[1] MIIT Key Laboratory of Aerospace Bearing Technology and Equipment, Harbin Institute of Technology, Harbin, China.
[2] State Key Laboratory of Robotics and System, Harbin Institute of Technology, Harbin, China.
[3] GUANGZHOU HAO ZHI INDUSTRIAL CO., LTD., Guangzhou, China

Abstract. Based on the rolling bearing vibration measurement principle in ISO standard, a nonlinear dynamic model of ball bearing is built and motion equations of the inner ring, outer ring, and rolling elements are derived by using Lagrange's equation. The ball bearing model includes the influence of waviness, rotational speed, external load, arbor supporting stiffness and arbor eccentricity. Ball bearing high-speed vibration tests are performed and used to verify the theoretical results. Simulated results showed that specific waviness orders produced the principal frequencies that were proportional to rotational speed. Rotational speed mainly affected the value of the natural frequency of the bearing system, and RMS (Root Mean Square) of the full band had a great fluctuation with the increase of rotational speed. In the experiment, spectrum and RMS of $2f_s$-30 kHz (f_s: the rotational frequency of inner ring/arbor) under high speed could include not only the influence of rotational speed but also principal frequencies produced by waviness, which could cover the part of requirements of the standard bearing vibration measurement.

Key words: rotational speed, ball bearing, vibration characteristics, frequency band, RMS.

1. Introduction

Bearing vibration measurement is an indispensable process of bearings quality inspection after their assembly. The rotational speed is one of the most crucial parameters for bearing vibration measurement. At present, rolling bearings-measuring methods for vibration have been standardized, for instance, BS ISO 15242, DIN ISO 15242, and GB/T 24610. Bearings vibration is usually measured with the outer ring being stationary and with inner ring turning at a constant rotational speed. The rolling bearing vibration measurement principle is illustrated in Fig. 1. The test ball bearing is usually subjected to an axial load and its default rotational speed is usually 30 rev/s. Default analyzed frequency range is 50–10 000 Hz, which is further divided into 50–300 Hz (low frequency band), 300–1800 Hz (medium frequency band), and 1800–10 000 Hz (high frequency band). However, the operating speed of modern high speed rotating machinery (for example, high speed motorized spindle, aero-engine) is much higher than 30 rev/s. To meet the speed requirements of modern bearing vibration measurement, bearing high-speed vibration test rigs are built. J.A. Wensing [1] replaced hydrodynamic bearings of the spindle with an aerospace bearing, and the standard test speed could be adjusted within 141.7 rev/s. Adamczak et al. [2] built the Anderometer STPPD bearing vibration test equipment, whose speed had improved to 60 rev/s. This equipment met the ISO design specifications.

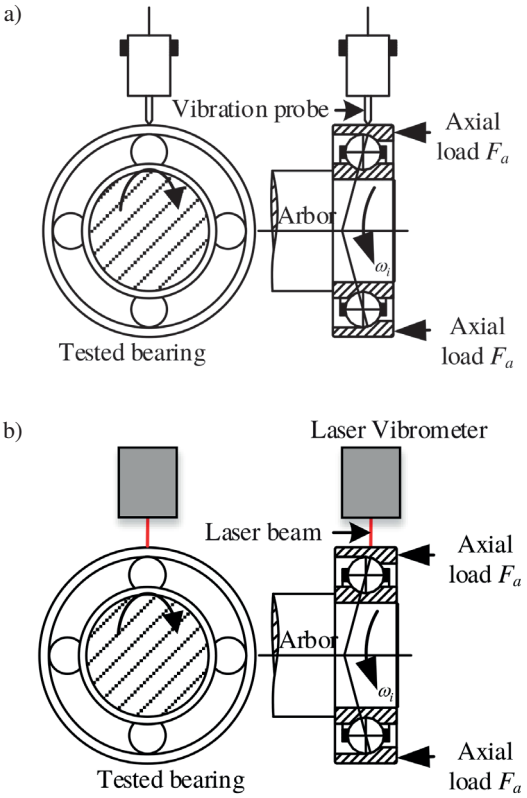

Fig. 1. Rolling bearing vibration measurement principle: a) contact measurement, b) noncontact measurement

Bearing vibration is the result of the displacements induced by error motion, which is a consequence of geometric imperfections of the diverse internal bearing surfaces. Waviness is an

*e-mail: lqwanghit@163.com

Manuscript submitted 2019-08-21, revised 2020-01-11, initially accepted for publication 2020-01-17, published in June 2020

important part of geometric imperfections and has a great influence on the characteristics of the bearing vibration response. There have been many studies that theoretically analyzed the relationship between waviness and bearing-rotor system vibration response spectrum. Reference [3, 4] built the relationship between the waviness order and principal frequencies by solving the static equations of bearing's inner ring, for example, principal frequencies $n \times N_b \times f_c$ (n: integer, N_b: number of rolling element, f_c: cage rotating frequency) were caused by outer raceway waviness order $n \times N_b \pm 1$ and principal frequencies $n \times N_b \times (f_s - f_c) \pm f_s$ were generated by inner raceway waviness order $n \times N_b \pm 1$ in the radial direction [4]. In [5], a rigid shaft supported by a pair of angular contact ball bearings was modeled as a three degree-of-freedom (3DOF) spring-mass system in the radial x and y directions and axial z-direction. The displacement response spectra characteristics due to the waviness of the outer race, inner race, and rolling element were analyzed. N. Tandon and A. Choudhury [6] presented a 3DOF dynamic model of the rotor-bearing system including the movements of the inner ring/shaft, outer ring/bearing house and cantilever portion/load in the radial x-direction. Simulated results showed that special frequencies caused by raceways waviness were related to outer/inner race defect frequency, and that the amplitudes of the spectral components owing to inner race waviness were much smaller than these of the outer race waviness. G.H. Jang and S.W. Jeong [7] considered the 2-angular motions and the 3-translational motions of the rotor and built a 5DOF nonlinear dynamic model for a rigid rotor supported by two or more ball bearings. They indicated that the waviness between the bearing components and the waviness between the supporting bearings could interact, and that the centrifugal force and gyroscopic moment of the ball affected the principle frequencies [8, 9]. Babu et al. [10] added the angular motion around the axial z-direction and a 6DOF model of a rigid rotor was built. The model predicted that the influence of inner race waviness on the vibration was larger as compared to that caused by the outer race and rolling element. Yaobin Zhuo et al. [11] simplified the shaft-bearing system to a 3DOF system, whose generalized displacements were three translational motions in the radial x-and y-directions, and axial z-direction. Simulated results revealed that the inner/outer raceway waviness would excite resonance when the order of waviness was equal or multiple to N_b. S.P. Harsha and C. Nataraj [12] used Lagrange's equation to obtain $(N_b + 2)$ second order, non-linear differential equations of N_b rolling elements and inner ring in the radial plane. They analyzed the influence of outer raceway waviness and the number of rolling elements on the dynamic behavior of a rotor-bearing system. Combination Lagrange's equation and component mode set (CMS) method, J.A. Wensing [1] considered that the outer ring was flexible. The effect of the waviness on the response of the outer ring was discussed without considering the motions of the inner ring. The statistical variations of vibration generated by the inner ring and ball waviness were much larger than for vibration generated by outer ring waviness.

Waviness also has an influence on the bearing vibration level. In [13], simulated results at the shaft speed of 15 rev/s showed that the vibration and acoustic response of bearing house would increase with the growth of waviness size. Adamczak and Zmarzły [14] carried out 6304-type bearing vibration on the Anderometer and studied the influence of raceway waviness on bearing vibration level. The experimental results at 30 rev/s indicated that an increase in the raceway waviness caused an increase in the vibration level. For medium bandwidth (300–1800 Hz), the influence was most prominent. Hiroyuki Ohta and Shiya Satake [15, 16] formed the vibration test of hybrid ceramic ball bearings, steel ball bearing and all-ceramic ball bearing on the Anderometer. The overall value of velocity was influenced by rotational speed, and it tended to increase with rotational velocities, whose range was from 8.3 to 30 rev/s. However, some studies had indicated that rotational speed was nonlinear with the dynamic performance of the bearing system [17–19]. Reference [18] showed that the curve of peak-to-peak of overall response-speed had a very rough appearance. Peak-to-peak of 58.3 rev/s was more than that of 166.7 rev/s.

In addition to the bearing models described above for the study of the effects of waviness on bearing vibrations, a series of bearing models have also been proposed in the study of bearing vibration responses with the localized defect. Sidra Khana et al. [20] built the 2 second-order, nonlinear differential equations for the inner ring/shaft and outer ring/housing in the radial x-direction. Sadok Sassi et al. [21] proposed a 3DOF system for the inner ring, ball and outer ring in the radial y-direction. N.S. Feng et al. [22], and Dick Petersen and Carl Howard [23] considered the movements of the inner and outer rings in the radial x- and y-directions and built the 4DOF nonlinear dynamic model for the bearing. N. Sawalhi and R.B. Randall [24] added a high frequency response of the bearing in the radial y-direction into the model of [22]. A 5DOF bearing-pedestal model was depicted. This bearing model was also used in [25]. Dick Petersen et al. [26] continued to increase the radial x-direction motion of a high frequency response into the model developed by [24]. A 6DOF bearing-pedestal model was described. Liu et al. [27] presented a 12DOF model of a rigid rotor-angular contact ball bearings system. This model included the three translational and three rotational displacements of the inner race/rotor, three translational displacements of the outer race of the right bearing, and three translational displacements of the outer race of the left bearing in the radial x-and y-directions, and axial z-direction.

In application, high speed has become the trend for rolling bearing vibration measurement, which will accompany the problem that the divided frequency bands at 30 rev/s may no longer be suitable for bearing high speed vibration measurement analysis. Therefore, it is necessary to study theoretically and experimentally the change of vibration characteristics of the bearing with rotational speed increases, which benefits to confirm the analysis frequency bandwidth of the evaluation method of rolling bearing high speed vibration measurement. However, the limitation of the above studies is to pay more attention to the influence of the special order of waviness of one of the bearing components on the bearing vibration response. The experimental and theoretical analyses for rolling bearing

vibration measurements are rarely performed at the same time, and for the individual bearing vibration measurement test, the test speed range can rarely cover the range from low speed to high speed.

In order to include the influence of rotational speed and satisfy the principle of rolling bearing vibration measurement, the ball bearing model and the derivation of the motion equations of the bearing components refer to [1, 12, 18, 28–30]. In this paper, $2N_b + 5$ differential equations of ball bearing are established by using Lagrange's equation. Waviness, operation parameters (rotational speed and load) and system parameters (arbor supporting stiffness and eccentricity) are considered. Then, considering bearing components waviness, the influence of rotational speed on response spectra and RMS of ball bearing vibration are analyzed theoretically, which are verified by bearing vibration experiments at low, medium and high speed. At last, the analysis frequency bandwidth at high speed is discussed.

2. Ball bearing vibration model considering rotational speed

The ball bearing is considered a spring-mass system as shown in Fig. 2. Bearing displacement error should be mainly caused by the inherent characteristics of bearing components, not the deformation of them. An appropriate axial load is sufficient to prevent slipping of the rolling elements relative to raceways and does not cause deformation of bearing components due to excessive load. Therefore, the outer ring is not bent, which is different from [1, 29]. The outer ring can move freely in the axial z-direction, which is different from [12, 18, 28, 30]. Based on the assumptions in [1, 12, 18, 28–30], the features of the ball bearing model are as follows:

(1) Ball bearing has a stable rotation. The angular velocity of the arbor (ω_i) around the z-axial is considered a constant value. The inner ring is assumed to be rigidly mounted on the arbor, so the inner ring and arbor have the same displacement and angular velocity, ω_i. The linear supporting stiffness in the radial x and y directions is K_{sx} and K_{sy}, respectively.

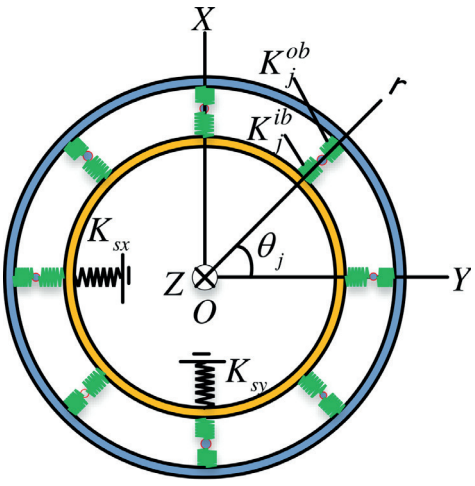

Fig. 2. Spring-mass model of ball bearing

(2) Except for local deformations between the outer-/inner-raceways and the rolling elements, the outer ring, inner ring, and rolling elements are rigid. The Hertzian theory of elasticity is used to calculate the local deformations. Rolling elements act as nonlinear contact springs as shown in Fig. 2. K_j^{ob} is the stiffness of the nonlinear spring connecting the jth rolling element and outer raceway, and K_j^{ib} is the stiffness of the nonlinear spring connecting the jth rolling element and inner raceway.

(3) The angle velocity of the cage (ω_c) is also assumed to be constant. The rolling elements are evenly distributed and guided by the cage. There is no slipping or sliding between the bearing components. The angular velocity of each rolling element about the z-axis is the same as the angular velocity of the cage, ω_c. The mass moment of inertia of a rolling element with respect to its mass center is neglected.

(4) The movements of the outer ring, inner ring, and rolling elements are in the radial XY plane and axial z-direction. The parameters that can describe the position of the bearing components are as follows: for the inner ring/arbor, translational DOFs are u_x^i in the radial x-direction and u_y^i in the radial y-direction; for the rolling elements, the movement of each rolling element in radial XY plane is described in a cylindrical coordinate and its position is written as $0.5D_m + u_{rj}^b$ (D_m: the pitch diameter), and the translational DOF of each rolling element in the axial z-direction is u_{zj}^b; for the outer ring, 3-translational DOFs are u_x^o, u_y^o and u_z^o in radial x-direction, radial y-direction, and axial z direction respectively.

(5) Because the damping due to friction and a small amount of lubrication and the structural damping are very small, these dampings are ignored.

Based on the relative positions of the jth rolling element, inner race and outer race in [1, 31], the instantaneous curvature center positions of raceways and the jth rolling element in the case where the rolling elements', inner ring's and outer ring's displacements are considered are shown in Fig. 3. Considering bearing components waviness, the instantaneous mutual approaches between the curvature centers of the jth rolling element and outer-/inner- raceways are respectively as follows (1) and (2) [1, 32].

$$\begin{aligned}
\delta_j^{ib} &= D_j^{ib} - D_0^{ib} + p_{ij} + u_{ij}\,,\\
D_0^{ib} &= (f_i - 0.5)\,D_b\,,\\
D_j^{ib} &= \sqrt{\left(D_{rj}^{ib}\right)^2 + \left(D_{zj}^{ib}\right)^2}\,,\\
D_{rj}^{ib} &= (f_i - 0.5)\,D_b \cos\alpha_0 - u_{rj}^i + u_{rj}^b\,,\\
D_{zj}^{ib} &= (f_i - 0.5)\,D_b \sin\alpha_0 + u_{zj}^b\,,\\
u_{rj}^i &= u_x^i \cos(\theta_j) + u_y^i \sin(\theta_j)\,;
\end{aligned} \tag{1}$$

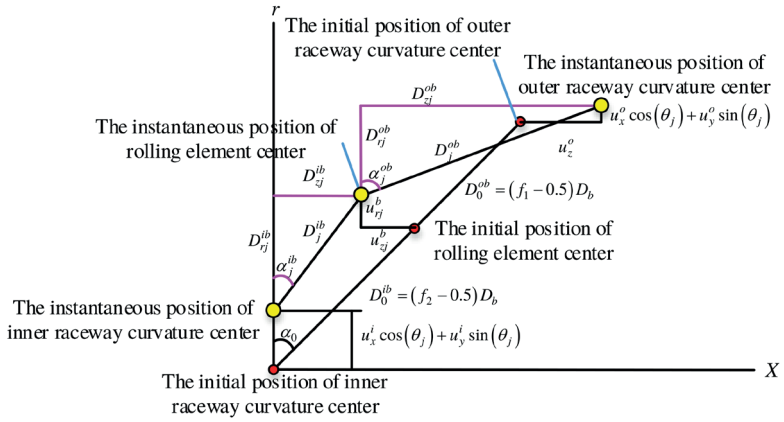

Fig. 3. Positional relationship between the jth rolling element center and raceways curvature center

$$\begin{aligned}
\delta_j^{ob} &= D_j^{ob} - D_0^{ob} + p_{oj} + u_{oj} \\
D_0^{ob} &= (f_1 - 0.5) D_b, \\
D_j^{ob} &= \sqrt{\left(D_{rj}^{ob}\right)^2 + \left(D_{zj}^{ob}\right)^2} \\
D_{rj}^{ob} &= (f_o - 0.5) D_b \cos\alpha_0 - u_{rj}^b + u_{rj}^o \\
D_{zj}^{ob} &= (f_o - 0.5) D_b \sin\alpha_0 - u_{zj}^b + u_z^o \\
u_{rj}^o &= u_x^o \cos(\theta_j) + u_y^o \sin(\theta_j),
\end{aligned} \tag{2}$$

where D_0^{ob} is the initial distance between the center of the curvature of the outer raceway and rolling element center. D_j^{ob} is the instantaneous distance between the center of the curvature of the outer raceway and the jth rolling element center. D_0^{ib} is the initial distance between the center of the curvature of the inner raceway and the rolling element center. D_j^{ib} is the instantaneous distance between the center of the curvature of the inner raceway and the jth rolling element center. p_{ij} and p_{oj} are the waviness of the inner raceway and outer raceway contacting with the jth rolling element. u_{ij} and u_{oj} are the waviness of the jth rolling element contacting with the inner raceway and outer raceway. D_b is the diameter of the rolling elements. f_i is the groove curvature coefficient of the inner race. f_o is the groove curvature coefficient of the outer race. α_0 is the initial contact angle. θ_j is the circumferential position of the jth rolling element.

The contact force between the jth rolling element and raceways can be generated only when there is a compression in the contact, that is, $\delta_j^{ib} > 0$ and $\delta_j^{ob} > 0$.

Lagrange's equation (3) deduces the differential equations of motion of the bearing components.

$$\partial\left(\partial T / \partial\{\dot{p}\}\right) \Big/ \partial t - \partial T / \partial\{p\} + \partial V / \partial\{p\} = \{f\}, \tag{3}$$

where T is the kinetic energy; V is the potential energy; $\{p\}$ is a vector for generalized degree-of-freedom; $\{f\}$ is a vector for generalized external forces.

The total potential energy includes the potential energy of the linear springs (K_{sx}, K_{sy}) and the potential energy of the nonlinear springs (K_j^{ib}, K_j^{ob}). The total potential energy is expressed as follows (4).

$$\begin{aligned}
V = &\frac{1}{2} K_{sy} \left(u_y^i\right)^2 + \frac{1}{2} K_{sx} \left(u_x^i\right)^2 + \\
&+ \sum_{j=1}^{N_b} \frac{2}{5} K_j^{ib} \left(\delta_j^{ib}\right)^{5/2} + \sum_{j=1}^{N_b} \frac{2}{5} K_j^{ob} \left(\delta_j^{ob}\right)^{5/2}.
\end{aligned} \tag{4}$$

The total kinetic energy is the sum of the translational and rotational kinetic energy of the arbor, inner ring, rolling elements, and outer ring. The total kinetic energy is expressed as (5):

$$T = T^r + T^i + T^b + T^o, \tag{5}$$

where T^r is the kinetic energy of the arbor. T^i is the kinetic energy of the inner ring. T^b is the kinetic energy of the rolling elements. T^o is the kinetic energy of the outer ring.

The contribution of the arbor contains the translational kinetic energy in the radial x and y directions and the rotational kinetic energy around the z axis. The kinetic energy expression of the arbor is (6).

$$T^r = \frac{1}{2} I^r \omega_{in}^2 + \frac{1}{2} m^r \left(\left(\dot{u}_x^i\right)^2 + \left(\dot{u}_y^i\right)^2\right), \tag{6}$$

where I^r is the moment of inertia of the arbor. m^r is the mass of the arbor.

The contribution of the inner ring includes the translational kinetic energy in the radial x and y directions and the rotational kinetic energy around the z-axis. The kinetic energy expression of the inner ring is (7).

$$T^i = \frac{1}{2} I^i \omega_{in}^2 + \frac{1}{2} m^i \left(\left(\dot{u}_x^i\right)^2 + \left(\dot{u}_y^i\right)^2\right), \tag{7}$$

where I^i is the moment of inertia of the inner ring. m^i is the mass of the inner ring.

The contribution of the jth rolling element is the total of the translational kinetic energy in the radial direction expressed by

a cylindrical coordinate, the translational kinetic energy in the axial z-direction, and the rotational kinetic energy around the z-axis. The kinetic energy expression of the jth rolling element is (8).

$$T_j^b = \frac{1}{2} m_j^b \left[\left(\dot{u}_{rj}^b \right)^2 + \left(\dot{u}_{zj}^b \right)^2 + \left(0.5 D_m + u_{rj}^b \right)^2 \omega_c^2 \right], \quad (8)$$

where T_j^b is the kinetic energy of the jth rolling element. m_j^b is the mass of the jth rolling element.

Then the kinetic energy of the N_b rolling element is as follow (9):

$$T^b = \sum_{j=1}^{N_b} T_j^b . \quad (9)$$

The contribution of the outer ring consists of the translational kinetic energy in the radial x and y directions and axial z-direction. The kinetic energy expression of the outer ring is (10).

$$T^o = \frac{1}{2} m^o \left((\dot{u}_x^o)^2 + (\dot{u}_y^o)^2 + (\dot{u}_z^o)^2 \right), \quad (10)$$

where m^o is the mass of the outer ring.

Generalized external forces include the imbalance force due to the eccentricity of the arbor center of mass along its geometric center of rotation exciting the inner ring/arbor in radial x and y directions and a constant axial load F_a acting on the outer ring in the axial z-direction.

For the generalized coordinates of the inner ring (u_x^i and u_y^i), the governing equations are (11). For the generalized coordinates of the jth rolling element (u_{rj}^b and u_{zj}^b), the governing equations are (12). For the generalized coordinates of the outer ring (u_x^o, u_y^o, and u_z^o), the governing equations are (13).

$$\begin{aligned}
&\left(m^i + m^r\right) \ddot{u}_x^i + K_{sx} u_x^i + \sum_{j=1}^{N_b} K_j^{ib} \left(\delta_j^{ib} \right)^{3/2} \partial \delta_j^{ib} / \partial u_x^i + \\
&\quad + \sum_{j=1}^{N_b} K_j^{ob} \left(\delta_j^{ob} \right)^{3/2} \partial \delta_j^{ob} / \partial u_x^i = \\
&\quad = \left(m^i + m^r\right) \times e \times \omega_i^2 \cos(\omega_i t), \\
&\left(m^i + m^r\right) \ddot{u}_y^i + K_{sy} u_y^i + \sum_{j=1}^{N_b} K_j^{ib} \left(\delta_j^{ib} \right)^{3/2} \partial \delta_j^{ib} / \partial u_y^i + \\
&\quad + \sum_{j=1}^{N_b} K_j^{ob} \left(\delta_j^{ob} \right)^{3/2} \partial \delta_j^{ob} / \partial u_y^i = \\
&\quad = \left(m^i + m^r\right) \times e \times \omega_i^2 \sin(\omega_i t),
\end{aligned} \quad (11)$$

$$\begin{aligned}
&m_j^b \ddot{u}_{rj}^b - m_j^b \times \left(0.5 D_m + u_{rj}^b \right) \times \omega_c^2 + \\
&\quad + K_j^{ib} \left(\delta_j^{ib} \right)^{3/2} \partial \delta_j^{ib} / \partial u_{rj}^b + \\
&\quad + K_j^{ob} \left(\delta_j^{ob} \right)^{3/2} \partial \delta_j^{ob} / \partial u_{rj}^b = 0,
\end{aligned} \quad (12)$$

$$\begin{aligned}
&m_j^b \ddot{u}_{zj}^b + K_j^{ib} \left(\delta_j^{ib} \right)^{3/2} \partial \delta_j^{ib} / \partial u_{zj}^b + \\
&\quad + K_j^{ob} \left(\delta_j^{ob} \right)^{3/2} \partial \delta_j^{ob} / \partial u_{zj}^b = 0,
\end{aligned}$$

$$\begin{aligned}
&m^o \ddot{u}_x^o + \sum_{j=1}^{N_b} K_j^{ib} \left(\delta_j^{ib} \right)^{3/2} \partial \delta_j^{ib} / \partial u_x^o + \\
&\quad + \sum_{j=1}^{N_b} K_j^{ob} \left(\delta_j^{ob} \right)^{3/2} \partial \delta_j^{ob} / \partial u_x^o = 0, \\
&m^o \ddot{u}_y^o + \sum_{j=1}^{N_b} K_j^{ib} \left(\delta_j^{ib} \right)^{3/2} \partial \delta_j^{ib} / \partial u_y^o + \\
&\quad + \sum_{j=1}^{N_b} K_j^{ob} \left(\delta_j^{ob} \right)^{3/2} \partial \delta_j^{ob} / \partial u_y^o = 0, \\
&m^o \ddot{u}_z^o + \sum_{j=1}^{N_b} K_j^{ib} \left(\delta_j^{ib} \right)^{3/2} \partial \delta_j^{ib} / \partial u_z^o + \\
&\quad + \sum_{j=1}^{N_b} K_j^{ob} \left(\delta_j^{ob} \right)^{3/2} \partial \delta_j^{ob} / \partial u_z^o = F_a ,
\end{aligned} \quad (13)$$

where e is the eccentricity of the arbor center of mass along its geometric center of rotation.

3. Simulation results

This research studies the velocity vibration response characteristic of the outer ring in the radial x-direction under an axial load. The main parameters of ball bearing are listed in Table 1. In the bearing industry, the periodicity of waviness is defined as a certain number of undulations per revolution (UPR). In the bearing dynamic analysis, the mathematical modeling of waviness is a superimposing of the sinusoidal functions as shown in (14) [1].

$$W(\theta) = \sum_{l=1}^{\infty} A_l \cos(l\theta + \varphi_l), \quad (14)$$

where l is the waviness order. The parameter A_l is the magnitude of the lth order. θ is the circumferential position. Expressions of θ of p_{ij}, p_{oj}, u_{ij} and u_j^o in (1) and (2) refer to [31]. The phase φ_l is uniformly distributed over the interval $[0, 2\pi]$.

Table 1
Main parameters of ball bearing

Number of the rolling element, N_b	17
Rolling element diameter, D_b	3.175 mm
Density of the rolling element, ρ_b	7800 kg/m^3
Pitch diameter, D_m	26 mm
Groove curvature coefficient of the outer race, f_o	0.535
Groove curvature coefficient of the inner race, f_i	0.545
Initial contact angle, α_0	15°

When analyzing the influence of the rotational speed on the bearing vibration response characteristics, the waviness parameters of the bearing component are considered at the same time. The waviness parameters of bearing components have the following characteristics:

(1) The waviness order is finite. According to JB/T 6642 (the standard of China), the outer raceway has a maximum order of 250. The inner raceway and rolling element waviness have a maximum order of 150.

(2) Fig. 4 showed the measurement waviness profile of the inner raceway of an angle contact rolling bearing and its discrete Fourier transform. The higher the order, the smaller the amplitude. The relationship between waviness amplitude and order is satisfied with the following (15) [1].

$$A_l = \frac{A}{l^s}, \tag{15}$$

where the parameter A is the magnitude of the first order. The exponent s is the amplitude decay for subsequent wave numbers.

(3) Considering the waviness of the inner raceway, outer raceway, and rolling elements simultaneously, the magnitude of the first order (A) and the their exponent (s) are the same.

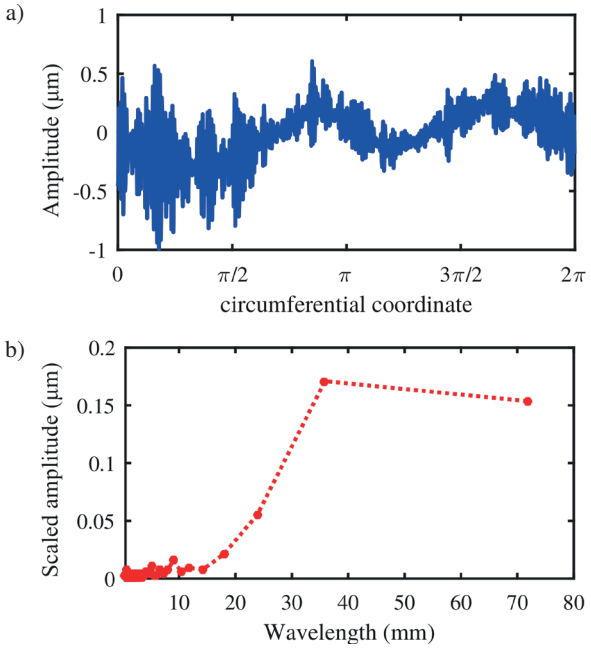

Fig. 4. a) Waviness measurement of the inner raceway of an angle contact rolling bearing. b) Discrete Fourier transform of waviness profile

The MATLAB ode23tb is used to solve the nonlinear differential equations ((11)–(13)). The calculation step size is 1×10^{-6} s. RMS of the amplitude of the outer ring velocity response will be used to evaluate the bearing vibration level. The response spectrum of the outer ring velocity response is obtained by FFT.

3.1. Characteristics of principal frequency caused by waviness. The relationship between the waviness order and the principal frequencies are listed in Table 2. Because both the cage rotation frequency (f_c) and the rolling element spinning frequency (f_b) are proportional to the inner ring/arbor rotation frequency (f_s), the principal frequencies are a function of the inner ring/arbor rotational frequency (f_s) and waviness order (l). Take waviness order 16 as an example. The principal frequency is satisfied by the function $y = 16 \times f_c - f_c$ as shown in Fig. 5. Except for the rotational speed of 800 rev/s, the amplitude of $16 \times f_c - f_c$ increases with the increase of f_s.

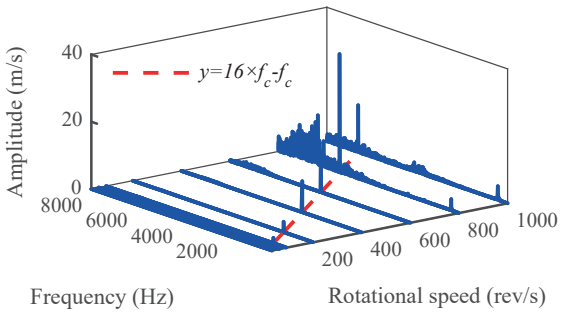

Fig. 5. Influence of rotational speed on the principal frequency in the radial x-direction (waviness order, amplitude, and phase are 16, 0.5 μm, and 0 rad, respectively)

3.2. Influence of rotational speed on bearing vibration considering bearing components waviness. When considering the bearing components waviness, the parameter A of p_{ij}, p_{oj}, u_{ij} and u_{oj} is 0.25 μm, the decay exponent s of p_{ij}, p_{oj}, u_{ij} and u_{oj} is 4, and the phase φ_l of p_{ij}, p_{oj}, u_{ij} and u_{oj} is 0 rad for each order. The rotational speed is varied in thirty steps in the range of 33.3–1000 rev/s. Fig. 6 shows the influence of rotational speed on spectra and RMS of the outer ring velocity response.

Table 2
Relationship between the waviness order and the principal frequencies (the rotational speed is 400 rev/s; $F_a = 60$ N; $K_{sx} = K_{sy}$ =3e7 N/m; $e = 0$ μm; waviness amplitude is 0.5 μm; the waviness phase is 0 rad)

Waviness order (l)		$n \times N_b$	$n \times N_b - 1$	$n \times N_b + 1$	Direction
The principal frequencies	Due to outer raceway waviness	$n \times N_b \times f_c \pm f_c$ $n \times N_b \times f_c$	$n \times N_b \times f_c - f_c$ –	$n \times N_b \times f_c + f_c$ –	Radial Axial
	Due to inner race waviness	$n \times N_b \times (f_s - f_c) \pm f_c$ $n \times N_b \times (f_s - f_c)$	$n \times N_b \times (f_s - f_c) + f_c$ –	$n \times N_b \times (f_s - f_c) - f_c$ –	Radial Axial
	Due to rolling element waviness	– $n \times f_b$	– –	– –	Radial Axial

where f_b is the rolling element spinning frequency.

Frequencies with larger amplitudes, which are represented by brighter colors in Fig. 6a), do not exceed 30 kHz. RMS of 0–30 kHz vs. Rotational speed curve and RMS of the full band vs. Rotational speed curve overlaps as shown in Fig. 6b). 0–30 kHz as shown by FB_1 (Frequency band) in Fig. 6a) are not affected by the rotational speed.

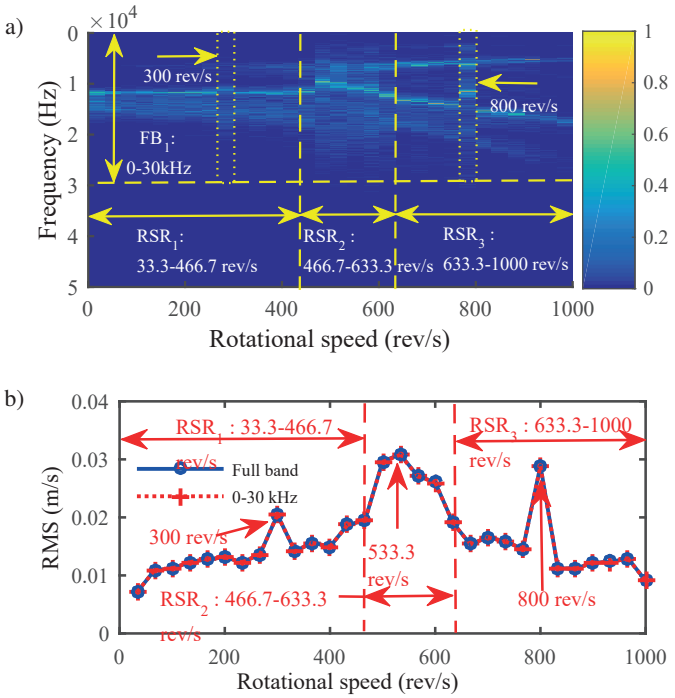

Fig. 6. Simulated results in the radial x-direction at $K_{sx} = K_{sy} =$ 3e11 N/m and $e = 0$ μm: a) Influence of rotational speed on velocity spectra of the outer ring. b) Influence of rotational speed on RMS of the outer ring velocity response

However, in FB_1, the distribution of frequencies with larger amplitudes changes with increasing of rotational speed. The rotational speed at which the frequency distribution changes in Fig. 6a) is consistent with the rotational speed at which the RMS is abrupt in Fig. 6b), namely 300 rev/s, 466.7 rev/s, 633.3 rev/s, and 800 rev/s. When the rotational speed range (RSR) is 33.3–466.7 rev/s (RSR_1 in Fig. 6a)), the distribution of frequencies with larger amplitudes is within 10 kHz–20 kHz and RMS in RSR_1 rises slowly with rotational speed increasing except for the rotational speed of 300 rev/s. The frequency bandwidth with larger amplitudes at 300 rev/s is a little bit wider and RMS of 300 rev/s is outstanding. In RSR_2, frequencies of larger amplitudes are dispersed in FB_1 and RMS increases from 466.7 rev/s to 533.3 rev/s but falls in 533.3–633.3 rev/s. In RSR_3, except for the rotational speed of 800 rev/s, the distribution of frequencies with larger amplitudes is bifurcated. RMS in RSR_3 declines slowly with rotational speed increasing but the rotational speed of 800 rev/s. This is because the condition of frequencies with larger amplitudes at 800 rev/s is similar to that of RSR_2. Therefore, RMS of 800 rev/s is larger than RMS of other speed in RSR_3.

4. Ball bearing high speed vibration test

Ball bearing vibration test was carried out on rolling bearing high speed vibration measurement rig, whose design guidelines were based on the GB/T 24610 (the standard of China). The process of establishing the test rig was in [33]. The method of the acceleration response measurement of the bearing outer ring was the contact type. This rolling bearing high speed vibration measurement rig complied with the principle of contact measurement as shown in Fig. 1a). Rotational speed was continuously variable by using the frequency transformer. The inner ring of tested bearing was driven directly by the high speed motorized spindle, whose maximum speed is 1000 rev/s. OptoMET Nova Series Digital Laser Doppler vibrometer is a noncontact sensor and replaces the contact sensor for measuring the outer ring vibration. This vibrometer can output displacement, velocity, and acceleration signals. Rolling bearing high speed vibration measurement rig with OptoMET Nova Series Digital Laser Doppler vibrometer conformed to the principle of bearing vibration measurement in Fig. 1b). The image of the noncontact and contact measurement of the rolling bearing high speed vibration measurement rig was shown in Fig. 7. The test bearing was high speed angle contact rolling bearings (7003 series made by FAG). Test speeds were 25/60/100/200/300/400/500/600 rev/s and an axial load was 60 N. DT9847 was used for data acquisition and the sampling frequency was 200 kHz. Lubricant oil was MOTOREX SPINDLE LUBE 68.

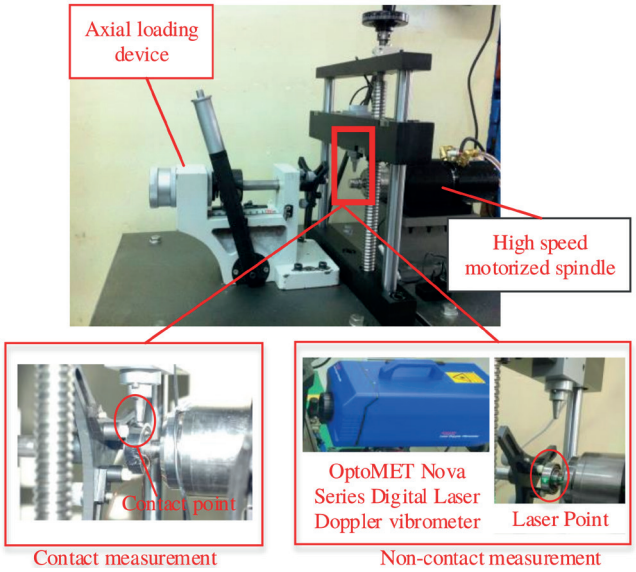

Fig. 7. Noncontact and contact measurement of the rolling bearing high speed vibration measurement rig

The test bearing is connected to the drive spindle and the loading tool. In addition to the bearing itself, the vibration of bearing outer ring is mainly superimposed on the vibration of the contact part of the bearing and the vibration generated by the interaction between parts of the system, such as the loading tool in contact with the outer ring, the inner ring mounted on drive

spindle's rotor, which is also supported by multiple bearings, as well as the influence of misalignment between the externally applied load and the spindle axis of rotation. Fig. 8 shows the frequency-domain comparison of contact and noncontact measurements at 400 rev/s. It can be seen from Fig. 8 that high multiple harmonic frequencies of the rotational speed are prominent in the response spectrum of the contact measurement, but not in the response spectrum of the noncontact measurement. This means that for the contact measurement, at high speed the influence of the system components on the vibration of the bearing itself is much more obvious than those of the noncontact measurement. Therefore, from the perspective of analyzing the vibration characteristics of the bearing itself, the noncontact measurement is far more suitable than the contact measurement to evaluate the bearing vibration level at high speed.

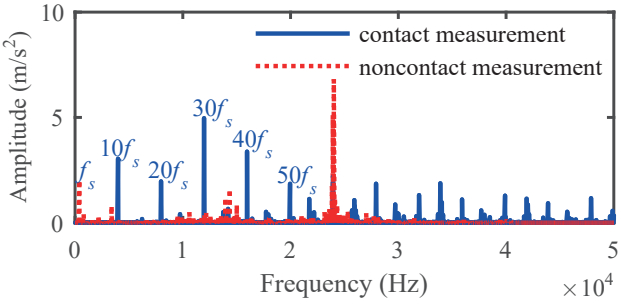

Fig. 8. Comparison of outer ring response spectra of contact and noncontact measurements at 400 rev/s

4.1. Validation of ball bearing model. At 400 rev/s, the velocity spectrum of the test bearing is shown in Fig. 9. Running speed is a little different from theoretical speed. There is a clear rotational frequency ($f_s \approx 399$ Hz) and a double frequency ($2f_s \approx 798.8$ Hz). Harmonics of rotation frequency ($3f_s$, $4f_s$, $5f_s$, $6f_s$) also exist. According to Table 2, there are principal frequencies, such as $N_b \times f_c + f_c$, $N_b \times (f_s - f_c) - f_c$ and $N_b \times (f_s - f_c) + f_c$.

However, in Fig. 9, there are $N_b \times f_c$ and $N_b \times (f_s - f_c)$, which are not in Table 2. This is because the outer ring is not tilted under an axial force in the theoretical calculation. However, in the experiment, the axial force is not aligned with the arbor axis and the outer ring is deflected, when an axial force is applied. These are the same as variable compliance vibration [34, 35]. This phenomenon can be confirmed by theoretical calculation. A 10 N radial load in the x-direction of the outer ring is applied. When the order of the inner and outer raceway waviness is N_b respectively, the simulated results show in Fig. 10. There are $N_b \times f_c$, $2 \times N_b \times f_c$ in Fig. 10a) and $N_b \times (f_s - f_c)$ in Fig. 10b). These show that the simplification of the bearing model is reasonable. On the other hand, the rolling bearing high speed vibration measurement rig can be used to measure the bearing vibration characteristics caused by waviness, which indicates that the bearing outer ring vibration response obtained by the experiment reflects the vibration characteristics of the individual bearings to some extent.

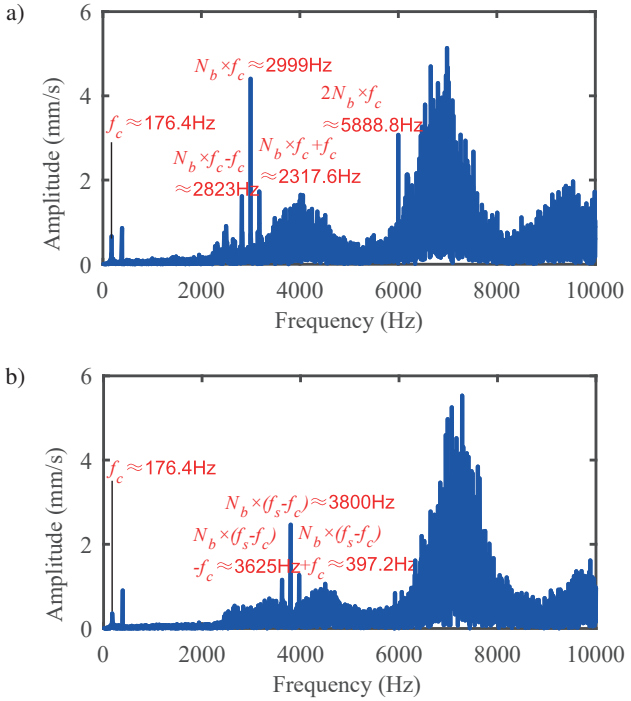

Fig. 10. Simulated velocity response spectra of the outer ring due to the inner and outer raceway waviness of order $l = N_b$ when the outer ring is subjected to 10 N x-radial force and 60 N z-axial force at 400 rev/s: a) Waviness in the outer raceway. b) Waviness in the inner raceway

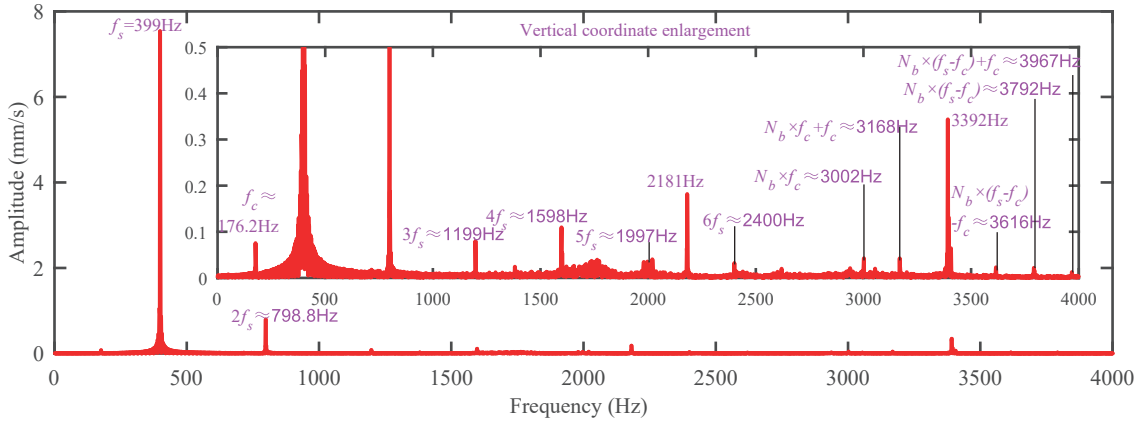

Fig. 9. Outer ring velocity response spectrum of at 400 rev/s on the rolling bearing high speed vibration measurement rig

4.2. Experimental results. As shown in Fig. 9, f_s and $2f_s$ are prominent. To eliminate the effects of arbor eccentricity and misalignment external load, the lowest cutoff frequency is $2f_s$. Fig. 11 shows the experimental results of spectra and RMS of the outer ring velocity response. Compared with Fig. 6, experimental and simulated results exhibit similar and different behaviors. Below 300 rev/s, the minimum frequency band, whose RMS is almost equal to RMS of the full band, is 0–30 kHz, as shown by FB_2 in Fig. 11a). After the rotational speed exceeds 300 rev/s, the difference value between RMS of 0–30 kHz and RMS of the full band gets larger. In FB_2, frequencies with larger amplitudes are mainly distributed around 15 kHz and around 25 kHz, which is different from the case where the distribution characteristic of the frequencies with larger amplitudes in FB_1 of Fig. 6a) change as the rotational speed increases. These frequencies with larger amplitudes, which are not affected by the rotational speed either, have been confirmed to be the natural frequencies of the bearing system [15, 16]. On the other hand, the tendency of RMS – rotational speed curve in Fig. 11b) is also similar to that of Fig. 6b). The differences are that rotational speed corresponding to maximum RMS in Fig. 11b) is 300 rev/s, while in Fig. 6b) this rotational speed is 533.3 rev/s, and that the value of RMS of the outer ring velocity response of the experimental results is significantly different from the RMS of the outer ring velocity response of the simulated results. Because the bearing model has simplified many of the effects of the test rig, compared to the experiment, the theoretically calculated outer ring vibration response is more reflective

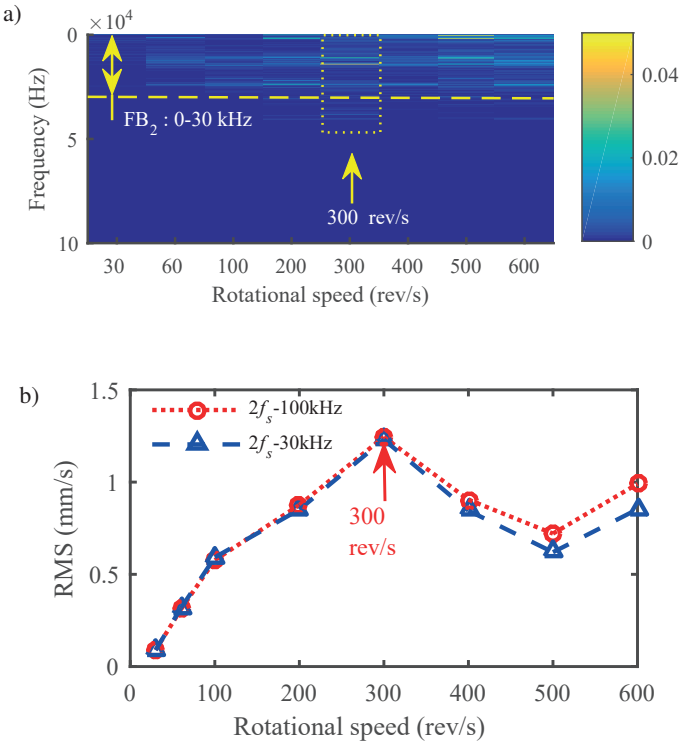

Fig. 11. Experimental results in radial x-direction: a) influence of rotational speed on spectra distribution of the outer ring velocity response (frequency band: $2f_s - 100$ kHz), b) influence of rotational speed on RMS of the outer ring velocity response

of the structural vibration of the individual bearing itself. When the bearing becomes part of a larger assembly, the measured bearing outer ring vibration response contains various vibration response originated each one of the parts of the system. The vibration of rotating rolling bearings is a complex physical phenomenon dependent on the conditions of operation, and a change in the rotational speed alone causes a strong change in the excitation of the dynamics of all parts of the system [17–19, 36]. These lead to significant differences between theoretical and experimental results.

Simulated and experimental results are of great importance to the high speed vibration evaluation of rolling bearings. Firstly, it is well known that one of the primary goals of bearing vibration measurement is the ability to evaluate the characteristics of waviness. In ISO 15242, at the default measurement speed (30 rev/s), the total analytical frequency (TF) band is from 50 Hz to 10 000 Hz, and it is also divided into three frequency bands: low frequency (LF) band is 50–300 Hz, medium frequency (MF) band is 300-1800 Hz, and high frequency (HF) band is 1800–10 000 Hz. Principal frequencies caused by waviness are proportional to rotational speed. Therefore, when tested speed is increased, all frequency bands have to be expanded in the same proportion theoretically to include the frequency characteristics caused by the waviness. Because these periodic frequencies are proportional to rotational speed, based on the characteristics of node frequencies of default analysis frequency band of 30 rev/s, the cut-off frequencies of these bands could be converted into parameters depended on the rotational speed, namely $2f_s - 300f_s$ (TF band), $2f_s - 10f_s$ (LF band), $10f_s - 60f_s$ (MF band) and $30f_s - 300f_s$ (HF band). Fig. 12 shows the experimental velocity response spectrum of 0–300 Hz at 25 rev/s. It also demonstrates that vibration characteristics caused by waviness can be reflected in 0–300 Hz. Therefore, the division of the frequency band will depend on the test speed. For the tested bearing, at high speed and low speed, $2f_s - 10f_s$ is helpful to analyze the frequency characteristics caused by the waviness order which is close to the number of rolling elements.

While the maximum cutoff frequency of TF at high speed will get great larger than that of 30 rev/s, for example, at 400 rev/s, the maximum cut-off frequency is 120 kHz, and the sampling frequency will be more than 240 kHz, which will be beyond the capability of most acquisition systems. The results of Fig. 6 and Fig. 11 show that the frequency bandwidth close to the vibration energy of the full band is limited. The cut-off frequency of FB_1 and FB_2 is much lower than 120 kHz. RMS of the frequency band is equal to that of the full band and reflects the influence of rotational speed on the bearing vibration level. On the other hand, according to [1] and the characteristics of the measured waviness in Fig. 4, the higher the order of waviness, the smaller its amplitude. The smaller the waviness amplitude is, the lesser the impact on the amplitude of the bearing vibration response [13]. Therefore, it is not necessary to satisfy the theoretical maximum cutoff frequency of TF. For example, for the tested bearing, the maximum cutoff frequency of TF could be 30 kHz at high speed.

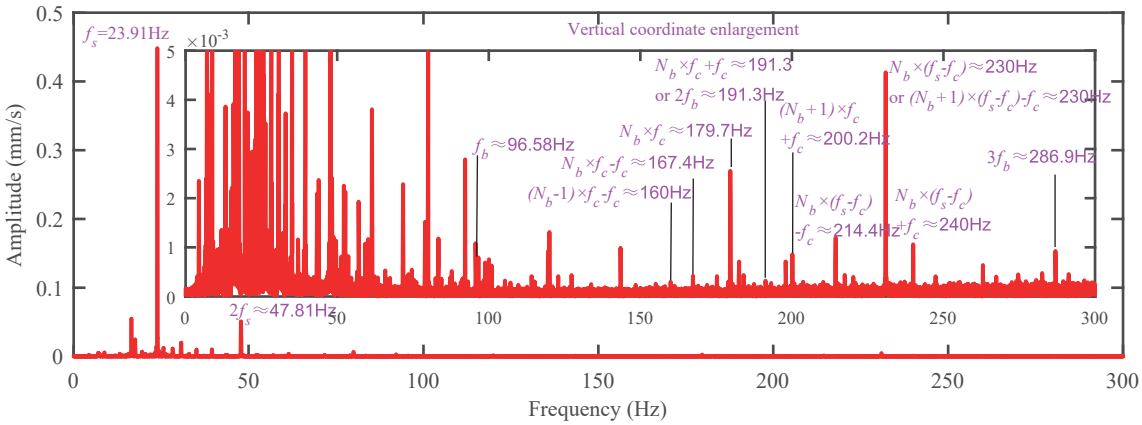

Fig. 12. Outer ring velocity response spectrum at 25 rev/s on BVT-5 (standard rolling bearing vibration measurement instrument made by HANGZHOU BEARING TEST & RESEARCH CENTER CO., LTD.)

5. Conclusions

According to the principle of bearing vibration measurement, a $2N_b + 5$DOF dynamic nonlinear model of the ball bearing is proposed. The mathematical bearing model involves the motions of the inner ring in the radial XY plane, the outer ring and rolling elements in the radial XY plane and axial Z direction. Bearing components waviness and rotational speed are considered into the ball bearing model. In the case where the inner ring raceway, outer ring raceway, and rolling elements waviness are considered at the same time, characteristics of response spectra and RMS of ball bearing vibration with the increase of the rotational speed are discussed. The vibration experiments of a high speed bearing are performed on the ball bearing high speed vibration measurement rig under low, medium and high speed. After eliminating the effects of the rotational frequency and its double frequency, simulated and experimental results showed that the width of the minimum frequency band whose RMS is almost equal to RMS of the full band is not influenced by the rotational speed, while RMS of the full band will fluctuate with the increase in rotational speed. This width of the minimum frequency band affects the choice of the sensor's performance parameters and vibration measurement mode and determines the analysis frequency bandwidth of the evaluation method of bearing high speed vibration measurement, which has a great significance for engineering applications.

Acknowledgements. The investigations were supported by the National Natural Science Foundation of China (Research Project U1637206) and the National key research and development program (Research Project 2018YFB0703804).

References

[1] J.A. Wensing, "On the dynamics of ball bearings", pp. 99–101, 47–97, 159–162, 16–18, Department of Mechanical Engineering, University of Twente, 1998.

[2] S. Adamczak, R. Domagalski, E. Sender, P. Zmarzły, and Ł. Gorycki, "Research methods and testing stand developed to examine vibrations generated by rolling bearing", *Diagnostyka*. 17 (1), 41–49 (2016).

[3] E. Yhland, "A linear theory of vibrations caused by ball bearings with form errors operating at moderate speed", *ASME. J. Tribol.* 114 (2), 348–359 (1992).

[4] K. Ono and K. Takahasi, "Theoretical analysis of shaft vibration supported by a ball bearing with small sinusoidal waviness", *IEEE Trans. Magn.* 32 (3), 1709–1714 (1996).

[5] Nizami Aktürk, "The effect of waviness on vibrations associated with ball bearings", *J. Tribol.* 121 (4), 667–677 (1999).

[6] N. Tandon and A. Choudhury, "A theoretical model to predict the vibration response of rolling bearings in a rotor bearing system to distributed defects under radial load", *J. Tribol.* 122 (3), 609–615 (2000).

[7] G.H. Jang and S.W. Jeong, "Nonlinear excitation model of ball bearing waviness in a rigid rotor supported by two or more ball bearings considering five degrees of freedom", *J. Tribol.* 124 (1), 82–90 (2002).

[8] G. Jang and S-W. Jeong, "Vibration analysis of a rotating system due to the effect of ball bearing waviness", *J. Sound Vibr.* 269 (3-5), 709–726 (2004).

[9] G.H. Jang and S.W. Jeong, "Analysis of a ball bearing with waviness considering the centrifugal force and gyroscopic moment of the ball", *J. Tribol.* 125 (3), 487–498 (2003)

[10] C.K. Babu, N. Tandon, and R.K. Pandey, "Vibration modeling of a rigid rotor supported on the lubricated angular contact ball bearings considering six degrees of freedom and waviness on balls and races", *J. Vib. Acoust.* 134 (1), 011006-011006-12 (2012).

[11] Y. Zhuo, X. Zhou, and C. Yang, "Dynamic analysis of double-row self-aligning ball bearings due to applied loads, internal clearance, surface waviness and number of balls", *J. Sound Vibr.* 333 (23), 6170–6189 (2014).

[12] S.P. Harsha and C. Nataraj, "The effect of surface waviness and number of rolling elements on the dynamic behavior of a rotor-bearing system", *Proceedings of the ASME 2007 International Design Engineering Technical Conferences and Computers and Information in Engineering Conference. Volume 1: 21st Biennial Conference on Mechanical Vibration and Noise, Parts A, B, and C. Las Vegas, Nevada, USA,* 2007, pp. 1755–1762.

[13] Y. Shao, P. Wang, and Z. Chen, "Effect of waviness on vibration and acoustic features of rolling element bearing", *ASME 2012 International Design Engineering Technical Conferences and Computers and Information in Engineering Conference. American Society of Mechanical Engineers, Chicago, Illinois, USA*, 2012, pp. 165–170.

[14] S. Adamczak and P. Zmarzły, "Influence of raceway waviness on the level of vibration in rolling-element bearings", *Bull. Pol. Ac.: Tech.* 65 (4), 541–551 (2017).

[15] H. Ohta and S. Satake, "Vibrations of hybrid ceramic ball bearings", *J. Sound Vibr.* 192 (2), 481–493 (1996).

[16] H. Ohta and S. Satake, "Vibrations of the all-ceramic ball bearing", *J. Tribol.* 124 (3), 448–460 (2002).

[17] H. Cao, F. Shi, Y. Li, B. Li, and X. Chen, "Vibration and stability analysis of rotor-bearing-pedestal system due to clearance fit", *Mech. Syst. Signal Proc.* 133, 106275 (2019).

[18] S.P. Harsha, "Nonlinear dynamic analysis of a high-speed rotor supported by rolling element bearings", *J. Sound Vibr.* 290 (1-2), 65–100 (2006).

[19] A. Sharma, N. Upadhyay, P. Kumar Kankar, and M. Amarnath, "Nonlinear dynamic investigations on rolling element bearings: A review", *Adv. Mech. Eng.* 10 (3), 1–15 (2018).

[20] S. Khanam, N. Tandon, and J.K. Dutt, "Multi-event excitation force model for inner race defect in a rolling element bearing", *ASME. J. Tribol.* 138 (1), 011106 (2016).

[21] S. Sassi, B. Badri, and M. Thomas, "A numerical model to predict damaged bearing vibrations", *J. Vib. Control*. 13 (11), 1603–1628 (2007).

[22] N.S. Feng, E.J. Hahn, and R.B. Randall, "Using transient analysis software to simulate vibration signals due to rolling element bearing defects", *Appl. Mech: Progress and Applications*. 689–694 (2002).

[23] D. Petersen and C. Howard, "Bearing defect size estimation for extended raceway defects", *INTER-NOISE and NOISE-CON Congress and Conference Proceedings. Institute of Noise Control Engineering*. 249 (5), 2787–2796 (2014).

[24] N. Sawalhi and R.B. Randall, "Simulating gear and bearing interactions in the presence of faults: Part I. The combined gear bearing dynamic model and the simulation of localised bearing faults", *Mech. Syst. Signal Proc.* 22 (8), 1924–1951 (2008).

[25] B. Dolenc, P. Boškoski, and Đ. Juričić, "Distributed bearing fault diagnosis based on vibration analysis", *Mech. Syst. Signal Proc.* 66–67, 521–532 (2016).

[26] D. Petersen, C. Howard, N. Sawalhi, A. Moazen Ahmadi, and S. Singh, "Analysis of bearing stiffness variations, contact forces and vibrations in radially loaded double row rolling element bearings with raceway defects", *Mech. Syst. Signal Proc.* 50–51, 139–160 (2015).

[27] J. Liu and Y. Shao, "Dynamic modeling for rigid rotor bearing systems with a localized defect considering additional deformations at the sharp edges", *J. Sound Vibr.* 398 (23), 84–102 (2017).

[28] P. Patra, V. Huzur Saran, and S.P. Harsha, "Non-linear dynamic response analysis of cylindrical roller bearings due to rotational speed", *Proceedings of the Institution of Mechanical Engineers, Part K: J. of Multi-body Dynamics*. 233 (2), 379–390 (2018).

[29] M. Tadina and M. Boltežar, "Improved model of a ball bearing for the simulation of vibration signals due to faults during run-up", *J. Sound Vibr.* 330 (17), 4287–4301 (2011).

[30] L. Cui, Z. Jin, J. Huang, and H. Wang, "Fault Severity Classification and Size Estimation for Ball Bearings Based on Vibration Mechanism", *IEEE Access.* 7, 56107–56116 (2019).

[31] X. Li, K. Yu, H. Ma, L. Cao, Z. Luo, and H. Li, et al., "Analysis of varying contact angles and load distributions in defective angular contact ball bearing", *Eng. Fail. Anal.* 91, 449–464 (2018).

[32] D.S. Shah and V.N. Patel, "Theoretical and experimental vibration studies of lubricated deep groove ball bearings having surface waviness on its races", *Measurement.* 129, 405–423 (2018).

[33] B. Yingcun, "Study on vibration characteristics of grease-lubricated bearings used in high-speed spindle", *Harbin Institute of Technology*. (2015) [in Chinese].

[34] R. Yang, L. Hou, Y. Jin, Y. Chen, and Z. Zhang, "The Varying Compliance Resonance in a Ball Bearing Rotor System Affected by Different Ball Numbers and Rotor Eccentricities", *J. Tribol.* 140 (5), 051101 (2018).

[35] H. Cheng, Y. Zhang, W. Lu, and Z. Yang, "Research on time-varying stiffness of bearing based on local defect and varying compliance coupling", *Measurement*. 143, 155–179 (2019).

[36] R. Serrato, M.M. Maru, and L.R. Padovese, "Effect of lubricant viscosity grade on mechanical vibration of roller bearings", *Tribol. Int.* 40 (8), 1270–1275 (2007).